Vernier-like super resolution with guided correlated photon pairs

Matteo Nespoli,[1,2,3] Hsi-Sheng Goan,[1,4,5,6] and Min-Hsiung Shih[2,3,6,*]

[1]*Department of Physics, National Taiwan University, No. 1, Sec. 4, Roosevelt Road, Taipei 106, Taiwan*
[2]*Nano Science and Technology Program, Taiwan International Graduate Program, Academia Sinica and National Taiwan University, Taipei, Taiwan*
[3]*Research Center for Applied Sciences, Academia Sinica, No. 128, Sec. 2, Academia Road, Nangang 115, Taipei, Taiwan*
[4]*Center for Quantum Science and Engineering and Center for Theoretical Sciences, National Taiwan University, No. 1, Sec. 4, Roosevelt Road, Taipei 106, Taiwan*
[5]*Department of Photonics, National Chiao Tung University, No. 1001, Daxue Road, East District, Hsinchu City, 300, Taiwan*
[6]*goan@phys.ntu.edu.tw*
[*]*mhshih@gate.sinica.edu.tw*

Abstract: We describe a dispersion-enabled, ultra-low power realization of super-resolution in an integrated Mach-Zehnder interferometer. Our scheme is based on a Vernier-like effect in the coincident detection of frequency correlated, non-degenerate photon pairs at the sensor output in the presence of group index dispersion. We design and simulate a realistic integrated refractive index sensor in a silicon nitride on silica platform and characterize its performance in the proposed scheme. We present numerical results showing a sensitivity improvement upward of 40 times over a traditional sensing scheme. The device we design is well within the reach of modern semiconductor fabrication technology. We believe this is the first metrology scheme that uses waveguide group index dispersion as a resource to attain super-resolution.

OCIS codes: (130.0130) Integrated optics, (270.0270) Quantum optics, (280.0280) Remote sensing and sensors.

References and links

1. K. J. Resch, K. L. Pregnell, R. Prevedel, A. Gilchrist, G. J. Pryde, J. L. O'Brien, and A. G. White, "Time-Reversal and Super-Resolving Phase Measurements," Phys. Rev. Lett. **98**(22), 223601 (2007).
2. C. Kothe, G. Björk, and M. Bourennane, "Arbitrarily high super-resolving phase measurements at telecommunication wavelengths," Phys. Rev. A **81**(6), 063836 (2010).
3. A. Chiruvelli and H. Lee, "Parity measurements in quantum optical metrology," J. Mod. Opt. **58**(11), 945–953 (2011).
4. L. Cohen, D. Istrati, L. Dovrat, and H. S. Eisenberg, "Super-resolved phase measurements at the shot noise limit by parity measurement," Opt. Express **22**(10), 11945–11953 (2014).
5. M. J. Holland and K. Burnett, "Interferometric detection of optical phase shifts at the Heisenberg limit," Phys. Rev. Lett. **71**(9), 1355–1358 (1993).
6. V. Giovannetti, S. Lloyd, and L. Maccone, "Advances in quantum metrology," Nat. Photonics **5**(4), 222–229 (2011).
7. Y. Gao, P. Anisimov, C. Wildfeuer, J. Luine, H. Lee, and J. P. Dowling, "Super-resolution at the shot-noise limit with coherent states and photon-number-resolving detectors," JOSA B **27**(6), 170–174 (2010).
8. P. M. Anisimov, G. M. Raterman, A. Chiruvelli, W. N. Plick, S. D. Huver, H. Lee, and J. P. Dowling, "Quantum Metrology with Two-Mode Squeezed Vacuum: Parity Detection Beats the Heisenberg Limit," Phys. Rev. Lett. **104**(10), 103602 (2010).
9. K. P. Seshadreesan, S. Kim, J. P. Dowling, and H. Lee, "Phase estimation at the quantum Cramér-Rao bound via parity detection," Phys. Rev. A **87**(4), 043833 (2013).
10. T. Nagata, R. Okamoto, J. L. O'brien, K. Sasaki, and S. Takeuchi, "Beating the standard quantum limit with four-entangled photons," Science **316**(5825), 726–729 (2007).
11. M. Z. Mousavi, H.-Y. Chen, S.-H. Wu, S.-W. Peng, K.-L. Lee, P.-K. Wei, and J.-Y. Cheng, "Magnetic nanoparticle-enhanced SPR on gold nanoslits for ultra-sensitive, label-free detection of nucleic acid

#253887 Received 17 Nov 2015; accepted 31 Dec 2015; published 6 Jan 2016

biomarkers," Analyst (Lond.) **138**(9), 2740–2748 (2013).
12. J. Hu, X. Sun, A. Agarwal, and L. C. Kimerling, "Design guidelines for optical resonator biochemical sensors," J. Opt. Soc. Am. B **26**(5), 1032 (2009).
13. C. Ciminelli, C. M. Campanella, F. Dell'Olio, C. E. Campanella, and M. N. Armenise, "Label-free optical resonant sensors for biochemical applications," Prog. Quantum Electron. **37**(2), 51–107 (2013).
14. F. Vollmer, D. Braun, A. Libchaber, M. Khoshsima, I. Teraoka, and S. Arnold, "Protein detection by optical shift of a resonant microcavity," Appl. Phys. Lett. **80**(21), 4057 (2002).
15. B. Bell, S. Kannan, A. McMillan, A. S. Clark, W. J. Wadsworth, and J. G. Rarity, "Multicolor Quantum Metrology with Entangled Photons," Phys. Rev. Lett. **111**(9), 093603 (2013).
16. A. Crespi, M. Lobino, J. C. F. Matthews, A. Politi, C. R. Neal, R. Ramponi, R. Osellame, and J. L. O'Brien, "Measuring protein concentration with entangled photons," Appl. Phys. Lett. **100**(23), 233704 (2012).
17. T. Claes, W. Bogaerts, and P. Bienstman, "Experimental characterization of a silicon photonic biosensor consisting of two cascaded ring resonators based on the Vernier-effect and introduction of a curve fitting method for an improved detection limit," Opt. Express **18**(22), 22747–22761 (2010).
18. X. Jiang, Y. Chen, F. Yu, L. Tang, M. Li, and J.-J. He, "High-sensitivity optical biosensor based on cascaded Mach-Zehnder interferometer and ring resonator using Vernier effect," Opt. Lett. **39**(22), 6363–6366 (2014).
19. S. Shabbir, M. Swillo, and G. Björk, "Synthesis of arbitrary, two-mode, high-visibility N -photon interference patterns," Phys. Rev. A **87**(5), 053821 (2013).
20. M. La Notte and V. M. N. Passaro, "Ultra high sensitivity chemical photonic sensing by Mach–Zehnder interferometer enhanced Vernier-effect," Sens. Actuators B Chem. **176**, 994–1007 (2013).
21. R. Ghosh, C. K. Hong, Z. Y. Ou, and L. Mandel, "Interference of two photons in parametric down conversion," Phys. Rev. A **34**(5), 3962–3968 (1986).
22. A. Fedrizzi, T. Herbst, A. Poppe, T. Jennewein, and A. Zeilinger, "A wavelength-tunable fiber-coupled source of narrowband entangled photons," Opt. Express **15**(23), 15377–15386 (2007).
23. R. Whittaker, C. Erven, A. Neville, M. Berry, J. L. O'Brien, H. Cable, and J. C. F. Matthews, "Quantum-enhanced absorption spectroscopy," 5 (2015).
24. V. M. N. Passaro, C. de Tullio, B. Troia, M. La Notte, G. Giannoccaro, and F. De Leonardis, "Recent advances in integrated photonic sensors," Sensors (Basel) **12**(11), 15558–15598 (2012).
25. V. Giovannetti, S. Lloyd, and L. Maccone, "Quantum-enhanced measurements: beating the standard quantum limit," Science **306**(5700), 1330–1336 (2004).
26. A. Z. Subramanian, P. Neutens, A. Dhakal, R. Jansen, T. Claes, X. Rottenberg, F. Peyskens, S. Selvaraja, P. Helin, B. DuBois, K. Leyssens, S. Severi, P. Deshpande, R. Baets, and P. Van Dorpe, "Low-Loss Singlemode PECVD Silicon Nitride Photonic Wire Waveguides for 532–900 nm Wavelength Window Fabricated Within a CMOS Pilot Line," IEEE Photonics J. **5**(6), 2202809 (2013).
27. Z. Weissman, E. Marom, and A. Hardy, "Very low-loss Y-junction power divider," Opt. Lett. **14**(5), 293–295 (1989).
28. D. T. H. Tan, K. Ikeda, P. C. Sun, and Y. Fainman, "Group velocity dispersion and self phase modulation in silicon nitride waveguides," Appl. Phys. Lett. **96**(6), 061101 (2010).
29. H. R. Philipp, "Optical Properties of Silicon Nitride," J. Electrochem. Soc. **120**(2), 295 (1973).
30. I. H. Malitson, "Interspecimen Comparison of the Refractive Index of Fused Silica," J. Opt. Soc. Am. **55**(10), 1205 (1965).
31. S. K. and I. N. N. Sultanova, "Dispersion Properties of Optical Polymers," http://przyrbwn.icm.edu.pl/APP/ABSTR/116/a116-4-42.html.

1. Introduction

In optical metrology the Rayleigh limit sets the ultimate bound for the resolution of an interferometer when a regular intensity read-out is employed. To overcome this boundary one has to increase the number of fringes for a given phase shift [1,2], or create a steeper response curves than the regular cosine output [3,4]. This can be achieved through preparation of non-classical states of light [5,6], unconventional read-out schemes [4,7,8], specialized interferometer setups [1] or measurements cascaded in either time or space [2]. Super-resolution occurs when the device responsivity, i.e. the derivative of the output variable with respect to the input, unknown phase, is increased beyond the classical bound. Super-resolution can be achieved independently of super-sensitivity [2,4,7,9], i.e. a decrease of the uncertainty in the measured variable below the shot noise limit (SNL). Contrary to super-resolution, super-sensitivity is believed to require entanglement [10]. To date implementation of super-resolved interferometers has relied on intensity readouts. In contrast the monitoring of the wavelength at which peaks or other sharp features occur in a device output, i.e. wavelength interrogation (WI), has established itself as the golden standard for integrated sensing [11–14]. Moreover, while examples of multi-wavelength super-resolution

#253887 Received 17 Nov 2015; accepted 31 Dec 2015; published 6 Jan 2016

schemes [15], as well as implementations of non-classical super-resolution in waveguide interferometers [16] exist, not much effort has been devoted to studying super-resolution in integrated platforms, where the large material and group index dispersions are regarded as formidable obstacles.

In this work we propose, develop and analyze a novel scheme that takes advantage of the group index dispersion in high-contrast waveguides to achieve super-resolution in the wavelength domain. Our method is based on the frequency correlation between photons created in a non-degenerate spontaneous parametric down-conversion process (SPDC) and is a close cognate of cascaded [2] and time-reversed super-resolved schemes [1], as well as of the optical Vernier effect [17,18]. With proper optimization, the wavelength responsivity of a conventional, integrated Mach-Zehnder interferometer (MZI) can be increased beyond the classical result. The uncertainty on the readout variable shows a degradation over the SNL consistent with previous results for cascaded measurements [2], yielding an appreciable improvement on the limit of detection (LoD) of a regular MZI. An example based on a well-established Silicon Nitride architecture is presented to showcase the power of the scheme we propose. Contrary to other schemes [2,4], our proposal is robust against device imperfections and does not require precisely setting the phase of the input light.

2. Cascaded phase measurement with photon pairs

The simplest way to achieve super-resolution in an interferometer is to build a readout curve as the product of the intensity of two or more outputs. Equivalently coincidence counting can be used [19]. Resch et al. [1] have provided an elegant explanation of the emergence of super-resolution in terms of time-reversal in the detection and preparation of path-entangled states. More simply, one can recall that an output of any periodicity can be constructed as a product of cosine curves, provided appropriate phase delays are applied. The probes can be spatially or temporally separated, with analogous results [2]. Let us now consider a MZI with a sensing arm of length L_s and a reference arm of length L_r. In the interest of our later discussion, let us consider the refractive indexes of the two arms, n_s and n_r, to be different as well as dependent on the probe light wavelength. An unknown refractive index change Δn that we wish to measure is inserted into the sensing arm (see Fig. 1a). The transmission function shift measured in a traditional WI of such a system [20] is given by

$$\begin{aligned} \Delta\lambda_{MZI} &= \bar{\lambda}_{\Delta n} - \bar{\lambda} = \frac{\bar{\lambda}\cdot L_s\cdot\Delta n}{\Delta L_{eff,\lambda}} \\ \Delta L_{eff,\lambda} &= L_s\cdot\left(n_{s,\lambda}-\frac{\partial n_{s,\lambda}}{\partial\lambda}\lambda\right)-L_r\cdot\left(n_{r,\lambda}-\frac{\partial n_{r,\lambda}}{\partial\lambda}\lambda\right), \end{aligned} \tag{1}$$

Where $\bar{\lambda}_{\Delta n}$ and $\bar{\lambda}$ are the wavelengths at which transmission maxima occur before and after the application of Δn, respectively, while $L_{,eff,\lambda}$ is the interferometer effective path difference.

Let us now drive the same interferometer with two probes of different wavelength. This can be thought as a frequency-domain implementation of the cascaded measurements mentioned above. The cascaded output will be given by the product of the transmission functions (see Fig. 1b)

$$\begin{aligned} I_{SPDC} &= \left|\tfrac{1}{2}\langle\psi_{MZI}|\left(|0,\lambda_1\rangle+e^{-i\varphi_1}|1,\lambda_1\rangle\right)\otimes\left(|0,\lambda_2\rangle+e^{-i\varphi_2}|1,\lambda_2\rangle\right)\right|^2 \\ &= \cos^2\left[\varphi_1/2\right]\cdot\cos^2\left[\varphi_2/2\right], \\ \varphi_i &= \frac{\pi}{\lambda_i}\left(L_s\cdot\left(n_{s,\lambda_i}+\Delta n\right)-L_r\cdot n_{r,\lambda_i}\right);\ i=1,2 \end{aligned} \tag{2}$$

where $\varphi_{1,2}$ are the phase delays between the two arms of the MZI for either probe.

#253887 Received 17 Nov 2015; accepted 31 Dec 2015; published 6 Jan 2016

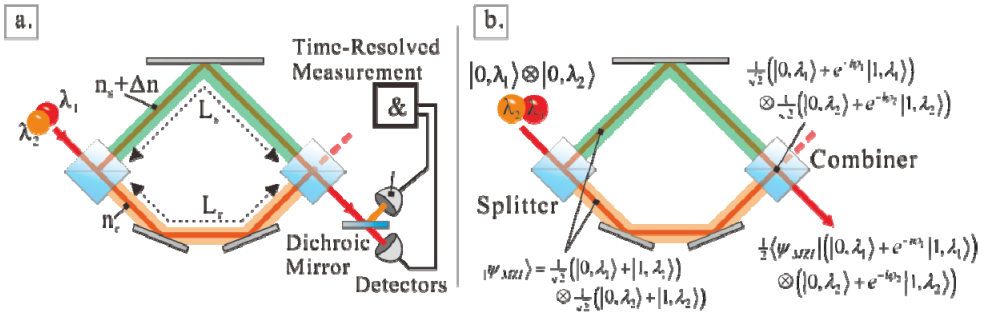

Fig. 1. (a) MZI driven by frequency correlated SPDC photon pairs. A dichroic mirror and two photon counters are used to register coincident detections. (b) Evolution of the two photons state inside the interferometer. The combiner acts as a time-reversed splitter. The joint detection probability is given by the projector of the splitter output state onto the split state $|\Psi_{MZI}\rangle$.

Choosing $\varphi_1 + \varphi_2 = \pi/2$, we could obtain a twofold increase in the number of fringes. This is equivalent to a two-component cascaded measurement. If we now look to implement WI, it becomes clear that we are dealing with a two-dimensional frequency space. This is not a problem in principle; however scanning two frequencies and extracting the phase information from the large data set produced would require unacceptable time and equipment overheads for any real implementation. To circumvent this, we impose a relation between the two wavelengths. We choose to use photon pairs generated through spontaneous parametric down-conversion (SPDC) [21]. Photon pair states offer an inherent frequency correlation suitable to our purpose,

$$\lambda_2 = \left(1/\lambda_p - 1/\lambda_1 \right)^{-1}, \tag{3}$$

where λ_p, λ_1 and λ_2 are the wavelengths of the pump, the signal and the idler, respectively. SPDC photon pairs also enjoy a strong time-correlation that is most amenable to coincidence counting, thus ensuring efficient and fast measurements at ultra-low power levels. In fact, for acceptable photon pair fluxes (10^6 to 10^8 photon pairs per second) the optical power passing through the sample is limited to about 50 pW. Lastly, a properly designed photon pair source lifts the requirement for a monochromator before the detectors, because the probes wavelengths can be precisely controlled by tuning the phase matching conditions within the source [22,23].

Having constrained the variation of one transmission function to the other, we have a system analogous to a Vernier-enhanced optical sensor [17], where we have substituted the dual sensor/filter system with two probes traversing a single device. In a Vernier sensor the filter response is not dependent on the unknown phase and has a fixed transmission curve. In our case, both probes pass through the measurement arm. However, due to the energy conservation relation for SPDC photons (3), once a wavelength is chosen for the first probe, the second one is automatically determined: when one transmission curve peaks move to longer (shorter) wavelengths due to a change in the unknown phase, the peaks of the second are forced to relocate to shorter (longer) wavelengths. The mechanism of "sliding scales" [20] at the heart of the Vernier effect is thus established. To understand the behaviour of the interferometer driven by photon pairs, we analyze the cascaded transmission function (2). This function exhibits two series of local maxima located at the midpoints between the maxima and minima of the single-probe transmission curves, respectively (see Fig. 2). Their envelopes are given by

#253887 Received 17 Nov 2015; accepted 31 Dec 2015; published 6 Jan 2016

$$\cos^4\left[\left(\varphi_1+\varphi_2\right)\Big/4\right] \quad ; \quad \sin^4\left[\left(\varphi_1+\varphi_2\right)\Big/4\right]. \tag{4}$$

The behavior of these envelopes and the responsivity one can extract from the relative position of their peaks depend dramatically on the group indexes.

In an interferometer whose arms are composed of a non-dispersive or weakly dispersive medium, e.g. air, the arguments in (4) are constants. In this situation the maxima within each series have a fixed value, independent of the wavelength. If the unknown refractive index Δn is varied, the relative height of the maxima changes, while their position remains unchanged. While slightly super-resolving, this scheme is hardly of any practical interest and it is in fact a non-optimal generalization of a two components cascaded measurement. Captivatingly, the same result is obtained if the refractive indexes have a linear dependence on the wavelength, i.e. if they exhibit chromatic dispersion but no group index dispersion.

In the presence of group index dispersion, as it is indeed the case of any integrated, solid-state interferometer, the results are a great deal more interesting. In general the probe phases will depend on the wavelength and the envelope functions in Eq. (4) will display maxima at positions dependent on the unknown index shift (Fig. 2). Using the phases dependence on the effective path difference (2) and energy conservation (3), it is straightforward to find the envelope shift

$$\Delta\lambda_{\mathrm{SPDC}} = \left(\frac{\bar{\lambda}_1^2}{\lambda_\mathrm{p}}\right)\cdot\frac{\Delta n\cdot \mathrm{L_s}}{\Delta \mathrm{L}_{\mathrm{eff},\lambda_1}-\Delta \mathrm{L}_{\mathrm{eff},\lambda_2}}. \tag{5}$$

Comparing this with expression (1), it is clear that the wavelength shift of the system driven by frequency correlated photon pairs can be much larger than the one obtained in the traditional case, provided the denominator in (5) can be minimized. This amplification of the responsivity is a form of super-resolution in the wavelength domain. A simple elaboration in terms of free spectral ranges (*FSR*) of an MZI, defined as

$$FSR = \frac{\lambda^2}{\Delta \mathrm{L}_{\mathrm{eff},\lambda}}, \tag{6}$$

yields the equivalent form, in which one can isolate the super-resolution factor $\mathrm{G_{SPDC}}$

$$\begin{aligned} \Delta\lambda_{\mathrm{SPDC}} &= \mathrm{G_{SPDC}}\cdot FSR_1\cdot\frac{\mathrm{L_s}\cdot\Delta n}{\bar{\lambda}_1} \\ \mathrm{G_{SPDC}} &= \frac{\Delta\lambda_{\mathrm{SPDC}}}{\Delta\lambda_{\mathrm{MZI}}} = \left(\frac{\bar{\lambda}_1}{\lambda_p}\right)\frac{FSR_2}{FSR_2-\left(\frac{\lambda_p}{\bar{\lambda}_1-\lambda_p}\right)^2\cdot FSR_1}, \end{aligned} \tag{7}$$

which is very similar to the well-known gain of Vernier sensors [17,20]. The configuration we describe can therefore be termed a Vernier-like effect for non-degenerate photon pairs. Instead of relying on multiple cascaded devices, super-resolution emerges from the group index dispersion within a single device. The super-resolution emerges from the relative phase lag between the photons in the highly dispersive interferometer. It is worth noting that our measurement does not require variable phase settings [1,2], nor number-resolving detectors [7].

#253887 Received 17 Nov 2015; accepted 31 Dec 2015; published 6 Jan 2016

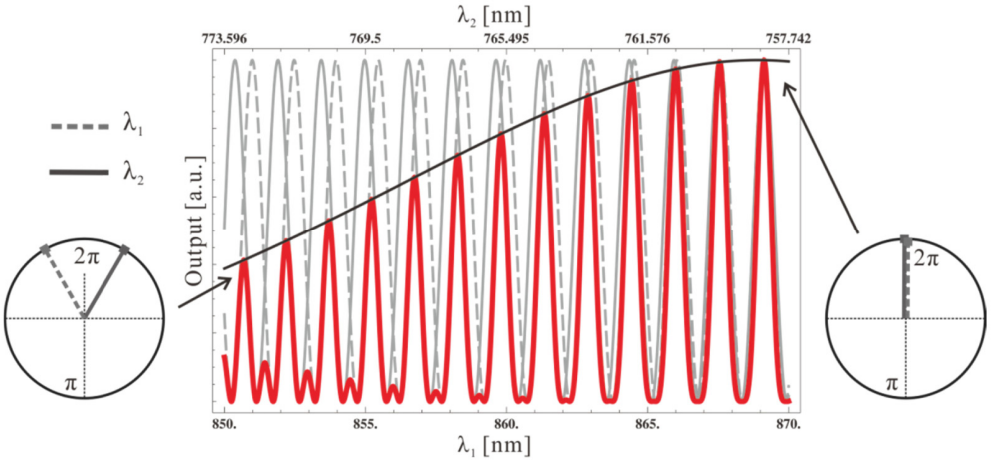

Fig. 2. Time-correlated output of the MZI. The cascaded output (red thick line) is enclosed by the Vernier-like curve (black thick line) defined in (4). The output intensity for the single probes as measured by single photon detectors are represented by solid and dashed gray thin lines. Representing the single probes as phasors whose position is regulated by (2) and (3), the Vernier-like envelope is defined as the single photon peaks go from being out of phase (left diagram) to in-phase (right diagram) as the wavelength of the SPDC source is scanned.

For a super-resolved scheme to yield a true advantage in terms of the smallest measurable shift (LoD), the uncertainty on the output variable need to be comparable to the one obtained in the regular readout or, at worst, degrade (increase) more slowly than G_{SPDC}. In the Vernier-like scheme such degradation stems from the envelope being much broader than the constituent peaks. Since the envelope cannot be measured directly, but rather be determined by fitting the peaks maxima to the expected output curve [17,18,24], an exact value of the uncertainty on $\delta(\Delta\lambda_{SPDC})$ is not readily calculated. A good estimate of its upper bound can be found using the average of the wavelengths of the single transmission peaks weighted by their relative intensity. Standard error propagation [25] yields the uncertainty

$$\delta\left(\Delta\lambda_{SPDC}\right) \cong \frac{1}{4}\sqrt{\frac{FSR_1}{FSR_2 - \left(\lambda_2^2 / \lambda_1^2\right) FSR_1}} \cdot \mathrm{SNL}, \tag{8}$$

which is higher than the shot noise limited value and grows with the square root of the super-resolving factor. This is very similar to the result obtained for spatially and temporally cascaded measurements [2] and yields an effective advantage in the measurement of the unknown index

$$\frac{\mathrm{LoD}_{SPDC}}{\mathrm{LoD}_{MZI}} \cong \frac{1}{4} \cdot \sqrt{\frac{FSR_2 - \left(\lambda_2^2 / \lambda_1^2\right) FSR_1}{FSR_1}}. \tag{9}$$

This result is similar to the one awarded by parity-based schemes [4,7].

3. Vernier-like super resolution in a silicon nitride waveguide interferometer

To demonstrate the application of the Vernier-like SPDC scheme in a realistic sensor, we consider a SPDC photon-pairs source similar to those presented in [22,23] operating at a pump wavelength of 405nm and producing non-degenerate photon pairs around 870nm and 750nm, respectively. The bandwidth of interest has been set to the interval between 730nm and 900nm. The material system we choose for the sensor is a thin film (220 nm) of silicon nitride (Si_3N_4) separated from a silicon carrier wafer by a 5μm silicon dioxide (SiO_2) buffer layer [26] and coated with 2μm of poly-methyl methacrylate (PMMA). To construct an MZI

#253887 Received 17 Nov 2015; accepted 31 Dec 2015; published 6 Jan 2016

we define fully etched rectangular waveguides of 600 nm width in the nitride layer. Y-shaped junctions [27] form the beam splitter and combiner, while two serpentine sections serve as the sensing and reference arm. The PMMA coating is selectively removed above the sensing arm to allow for interaction with liquid-phase samples. It is important to notice that this device is well within the current fabrication capabilities of any integrated optics research laboratory and it has in fact been realized a number of times in recent years. A scheme of the sensor is shown in Fig. 3a. In such an integrated system dispersion is dominated by confinement effects [28] and depends strongly on the waveguide geometry. For this reason, we used a finite element solver (Comsol® 3.5) to compute the effective index of the waveguides in the interferometer arms. A water coating was considered for the sensing arm at rest, i.e. $\Delta n = 0$. Experimentally derived Sellmeier equations [29–31] were fed into the program for all materials involved.

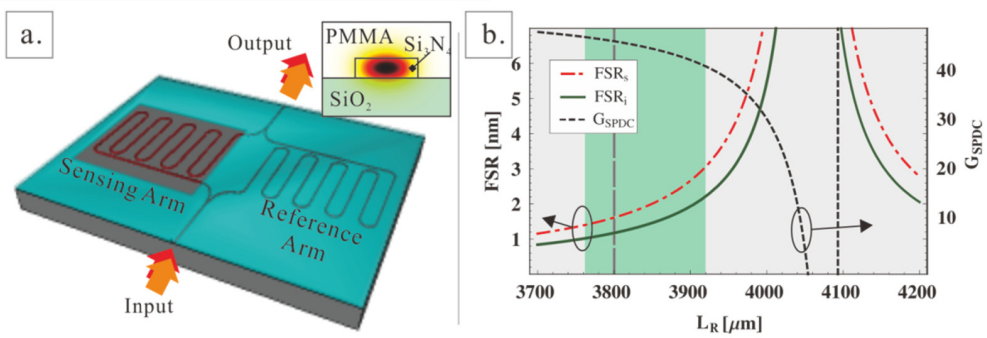

Fig. 3. (a) Scheme of the integrated, silicon nitride based, MZI sensor considered. The inset shows a simulated mode profile of the waveguides. (b) Calculated *FSR*s for the two probes (left scale) and super-resolving factor G_{SPDC} (right scale) for a measurement arm length of 4mm. The ideal working range (central green shaded area) is located between a region with very short *FSR* that would require an unrealistically narrow input bandwidth (left shaded area) and one where the *FSR* diverges to very large values (right shaded area), yielding very broad output peaks and a Vernier-like envelope that falls outside the chosen bandwidth of our waveguide system. The expected G_{SPDC} at the chosen working point (vertical gray dashed line, $L_r = 3.8$mm) is approximately 45.

Similar simulations were also used to calculate the waveguide sensitivity, i.e. the ratio between the effective index change and the sample index. From the simulation results the group index and FSRs for each wavelength were computed as functions of the lengths of the sensing and reference arms. The simulations also confirmed that our system remains single mode and guiding over the whole bandwidth. In order to optimize the sensor structure we set the sensing arm to 4mm and choose the length L_r of the reference arm to obtain the largest possible responsivity while yielding a manageable FSR. We choose a reference arm length of 3.8mm, which yields an *FSR* of about 1.5nm (see Fig. 3b), and calculate the transmission functions for a regular and a Vernier-like WI schemes.

Results for an index shift $\Delta n = 10^{-4}$ refractive index units (RIU) are shown in Fig. 4a. The wavelength shift obtained for the SPDC photon pairs is about 7.15nm, compared to a 0.15nm shift for the same MZI operated with a regular laser (Fig. 4b). As expected, the super-resolution factor is much larger than the one obtained in other two probes schemes [2,16]. To estimate the improvement in LoD we need to take into account the degradation of the wavelength uncertainty (8) as well as an experimentally realistic wavelength resolution. Assuming the wavelength can be set in steps of 0.1nm, the envelope center can be determined within ~0.17nm, so that the index LoD is approximately 2.5×10^{-6} RIU for the Vernier-like interrogation scheme, compared to about 6.7×10^{-5} RIU for a regular WI. A calculation accounting for wavelength dependent losses [26], detector efficiencies, device

#253887 Received 17 Nov 2015; accepted 31 Dec 2015; published 6 Jan 2016

imperfections and source non-idealities yields a slightly different output curve, but does not influence our core result. This is a major advantage of our scheme over parity and zero-photon based readouts, where both the signal and the output noise degrade rapidly in less than ideal devices [4,7]. This suggests our scheme can be feasibly implemented in practical sensors.

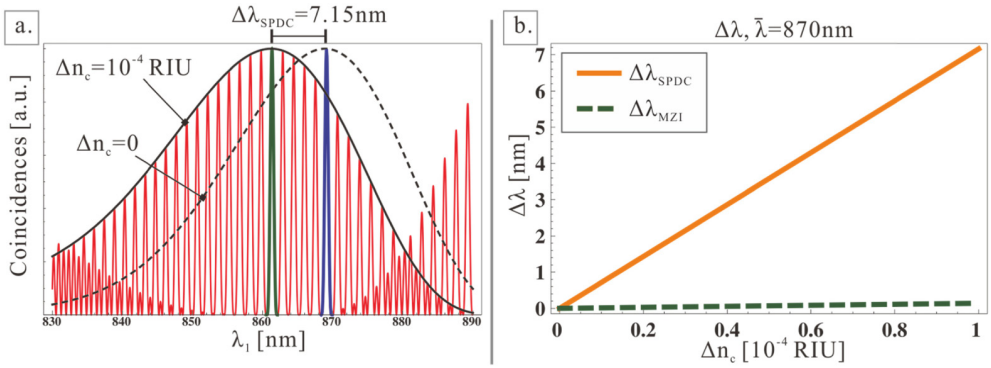

Fig. 4. Numerical results for the Vernier-like joint measurement. (a) Output curves for the MZI at rest and for a refractive index shift $\Delta n = 10^{-4}$ are shown. The wavelength responsivity is 71.5μm/RIU, opposed to the responsivity of a regular, single wavelength readout of 1.5μm/RIU. Central peaks in the envelope function before and after the index shift are highlighted. (b) Comparison between the peak wavelength responsivity for the integrated MZI driven by a single probe (dashed green line) and the Vernier-like, SPDC-based responsivity in the same device (orange full line).

4. Conclusions

In this work we have presented a proposal for an ultra-low power, super-resolved, Vernier-like measurement scheme in a MZI using SPDC photon pairs. Our approach is based on WI and, with proper optimization of the source, does not require wavelength- or number resolving detectors. We have described the emergence of super-resolution in our scheme and presented numerical results for its implementation in an integrated sensor based on silicon nitride waveguides. We have shown an almost 50 times improvement in the wavelength shift responsivity and a twentyfold decrease in the LoD. We believe our proposal is the first example of using waveguide dispersion as a resource. It is likely dispersion engineering can be applied to quantum-enhanced metrology in ways that are more powerful than the one described here. We hope this work will spark interest in researching these issues.

Acknowledgments

MHS acknowledge support from the Ministry of Science and Technology (MOST), Taiwan and NSC under Grant No. 102-2112-M-001-019-MY3. HSG acknowledge support from the MOST under Grant No. 103-2112-M-002-003-MY3, and from NTU under Grants No. 104R891402.

#253887 Received 17 Nov 2015; accepted 31 Dec 2015; published 6 Jan 2016